SIMULTANEOUS LOCALIZATION, MAPPING AND CHARACTERIZATION AROUND A SMALL BODY USING A MONOCULAR CAMERA

Felice Piccolo[1*], Paolo Panicucci[1] and Francesco Topputo[1]; [1]Politecnico di Milano, Via La Masa 34, Milan, Italy, [*][felice.piccolo@polimi.it]

Abstract. *The exploration of small bodies is one of the frontiers of space exploration. With the advent of small spacecraft, the number of proposed missions is increasing. Innovative mission concepts for the large-scale exploration of the small body population are being studied. Increased spacecraft autonomy is one of the enabling technologies for such missions. The objective of this work is to assess the feasibility of simultaneously estimating the state of the spacecraft, a set of landmarks on the target and the asteroid characteristics considering a single spacecraft equipped with a monocular camera.*

Introduction. The exploration of minor bodies has recently gained significant interest in the space community because of their importance from the scientific and technological point of view. Asteroids are remnants from the formation period of the Solar System, and as such they offer a unique opportunity to understand the history and future evolution of inner planets. Furthermore, they store a vast amount of precious materials that could be used both on Earth and in space.[1] The diversity of small bodies in the Solar System has been proven by the dedicated space missions of the last two decades. More missions are planned in the near future, some of which are specifically designed for small spacecraft (e.g. M-ARGO[2]). Furthermore, innovative mission concepts are being developed to achieve large scale exploration of asteroids in the Solar System.[3] However, such missions require a significant increase in spacecraft autonomy with respect to the current paradigm, which is based mostly on ground-in-the-loop monitoring and operations. Not only this increases the mission costs, but it also limits the scientific return of the mission because of the lack of real-time control, that limits the spacecraft to safe trajectories. Furthermore, missions to small bodies are often characterized by a large uncertainty about the characteristics of the target (e.g., shape and rotation), especially when considering small asteroids. Currently, considerable effort by ground operators is needed to characterize the target body and navigate the spacecraft around it.[4]

Simultaneous Localization and Mapping. The problem of building a consistent map of the environment while at the same time estimating the pose of a mobile platform is known in the robotic community as Simultaneous Localization and Mapping (SLAM). Theoretically, this kind of algorithm could enable spacecraft operations around completely unknown bodies. In the last decades many SLAM solutions have been proposed. They can be mainly divided in two categories: visual SLAM, that is based on optical images, and lidar SLAM, that instead relies on lidar sensors.[5] Visual SLAM has gained significant popularity because of the improvements in computer vision algorithms. For space applications, cameras are among the most used sensors since they require low power, mass and volume but at the same time provide significant information about the surrounding environment. Different variations of SLAM algorithms exist for monocular, stereo and RGB-D cameras. However, the depth information provided by stereo and depth cameras is typically available only at limited distance (meters, or tens of meters), thus they are not applicable when considering the typical range of spacecraft orbits, even in the case of close proximity operations around small bodies. Therefore, monocular cameras have to be considered. Visual SLAM algorithms can be divided in two main categories: direct and indirect.[6] The former is based on direct image alignment by minimization of the photometric error. The latter instead relies on processing images to obtain a set of distinct features that are tracked or matched across subsequent frames. Hybrid approaches also exist, that are generally based on direct image alignment in subsequent frames and feature extraction only on a subset of images.[7] Typical SLAM algorithms estimate the environment map and the pose of the robot, which is composed by its position and orientation. However, the estimated state vector can be enlarged to include other quantities of interest, such as the probe velocity.

Methodology. In this work, a spacecraft operating in close proximity of an asteroid is considered. An Extended Kalman Filter (EKF) is used to estimate the position and velocity of the satellite with respect to the target, its gravitational parameter and a map of the asteroid, composed by a set of discrete landmarks. The EKF dynamical model accounts only for the asteroid's gravitational attraction. The position and velocity of the spacecraft are estimated in an inertial reference frame, while the landmark positions in an asteroid-fixed reference frame. In this preliminary study the rotational state of the asteroid is assumed to be known. Furthermore, it is assumed that the initial position of the spacecraft is known, and that a preliminary estimate of the asteroid's gravitational parameter is available to initialize the EKF. Finally, a star tracker is assumed to be available to estimate the spacecraft attitude with respect to the inertial reference frame. A feature-based SLAM approach is considered. The EKF is fed by the line-of-sight measurements obtained by detecting and tracking features across subsequent frames. The image processing pipeline is simulated employing high-fidelity images rendered using Blender* and a procedural minor body generator tool.[8] An example of the resulting simulated images is shown in Fig-

*http://www.blender.org - Last accessed on 17/09/2022.

ure 1, which is obtained from a shape model of asteroid (101955) Bennu, to which boulders of various dimensions are added. The image processing pipeline works as follows. First, SURF features are extracted from the image. The 100 strongest features are selected and are matched with those from the previous frame. Known features, i.e. features that had already been matched previously, are used to update the EKF solution, while newly matched features are used to initialize new landmarks in the EKF map. Landmarks are represented using the inverse depth parametrization, a formulation that improves the linearity of the measurement equations.[9] To improve the quality of the produced map and to avoid excessive growth of the EKF state vector, features that have been matched less than a user-specified amount of times are removed from the state vector.

Results. The simulation scenario reproduces that of a spacecraft in the characterization phase of an asteroid similar to Bennu. The spacecraft is initially positioned at a distance of about 3 km from the asteroid. The trajectory in the asteroid-fixed frame is represented in Figure 2. An ideal camera pointing towards the centre of the asteroid is assumed, but a representative star tracker error of 10 arcseconds on each axis is considered. The simulation spans one rotational period of the asteroid, which corresponds to about 4.3 hours. The simulation is stopped after one period because no loop closure mechanisms have been implemented yet in the image processing architecture. Images are taken at one-minute intervals. The simulated camera is characterized by a 1024x1024 resolution, 100 mm focal length and 8 degrees field of view. The gravitational parameter of the asteroid is set to 5.2329 $\frac{\mathrm{m}^3}{\mathrm{s}^2}$, and its standard deviation at the beginning of the simulation to the 10% of the true value. In the EKF, the feature location error in the image is assumed to be represented by a Gaussian noise with 0 mean and a standard deviation of 2 pixels. As for the landmarks, the standard deviation employed for the initialization of the inverse depth parameter is set to $5 \times 10^{-5} \frac{1}{\mathrm{m}}$, which corresponds to about 500 m at a distance of 3 km. Finally, the number of minimum matches to keep a landmark in the EKF map is set to 8. The process noise matrix is currently fixed, with a noise standard deviation of 0.01 m for the position and $10^{-5} \frac{\mathrm{m}}{\mathrm{s}}$ for the velocity. The results for the position and velocity are presented in Figure 4. The estimation of the velocity performs well. The error is very small and well within the formal uncertainty of the EKF. As for the position, the error is also small, in the order of 0.1% of the spacecraft range, but some inconsistency with respect to the formal covariance is observed. This may be due to the fact that the image-to-image feature matching produces an accumulation of the error of the feature position over time that is not accurately captured by the formal covariance. The gravitational parameter estimation error is presented in Figure 3. The performance is consistent, and the initial error is significantly reduced during the simulation, despite its limited time span. Finally, the performance of the shape reconstruction is shown in Figure 5. The histogram shows the probability distribution of the reconstruction error, computed as the minimum distance between the reconstructed landmark positions and the true shape model. The error is shown as percentage with respect to Bennu's mean radius (262.5 m), and its mean value is 1.69% (4.44 m).

Conclusion. This work confirms that SLAM algorithms are suitable for spacecrafts operating in proximity of an asteroid. Even a single spacecraft equipped with a monocular camera manages to obtain a good localization and mapping accuracy. Future work will be focused on expanding the estimation process to the asteroid rotational state and on improving the image processing pipeline with the capability to perform loop closure. Furthermore, alternatives to the EKF formulation and to the feature matching algorithm used here will be investigated (e.g., the Kanade-Lucas-Tomasi feature tracking algorithm[10]).

References.

[1] A. M. Hein, R. Matheson, and D. Fries, "A techno-economic analysis of asteroid mining," *Acta Astronautica*, vol. 168, pp. 104–115, 2020.

[2] F. Topputo, Y. Wang, C. Giordano, *et al.*, "Envelop of reachable asteroids by M-ARGO CubeSat," *Advances in Space Research*, vol. 67, no. 12, pp. 4193–4221, 2021.

[3] A. Slavinskis, P. Janhunen, P. Toivanen, *et al.*, "Nanospacecraft fleet for multi-asteroid touring with electric solar wind sails," in *2018 IEEE Aerospace Conference*, pp. 1–20, IEEE, 2018.

[4] O. Barnouin, M. Daly, E. Palmer, *et al.*, "Digital terrain mapping by the osiris-rex mission," *Planetary and Space Science*, vol. 180, p. 104764, 2020.

[5] C. Cadena, L. Carlone, H. Carrillo, *et al.*, "Past, present, and future of simultaneous localization and mapping: Toward the robust-perception age," *IEEE Transactions on robotics*, vol. 32, no. 6, pp. 1309–1332, 2016.

[6] T. Taketomi, H. Uchiyama, and S. Ikeda, "Visual slam algorithms: A survey from 2010 to 2016," *IPSJ Transactions on Computer Vision and Applications*, vol. 9, no. 1, pp. 1–11, 2017.

[7] S. H. Lee and J. Civera, "Loosely-coupled semi-direct monocular slam," *IEEE Robotics and Automation Letters*, vol. 4, no. 2, pp. 399–406, 2018.

[8] C. Buonagura, M. Pugliatti, and F. Topputo, "Procedural Minor Body Generator Tool for Data-Driven Optical Navigation Methods," in *6th CEAS Specialist Conference on Guidance, Navigation and Control-EuroGNC*, pp. 1–15, 2022.

[9] J. Civera, A. J. Davison, and J. M. Montiel, "Inverse depth parametrization for monocular SLAM," *IEEE transactions on robotics*, vol. 24, no. 5, pp. 932–945, 2008.

[10] B. D. Lucas and T. Kanade, "An iterative image registration technique with an application to stereo vision," *Proceedings of the 7th International Joint Conference on Artificial Intelligence*, vol. 81, 1981.

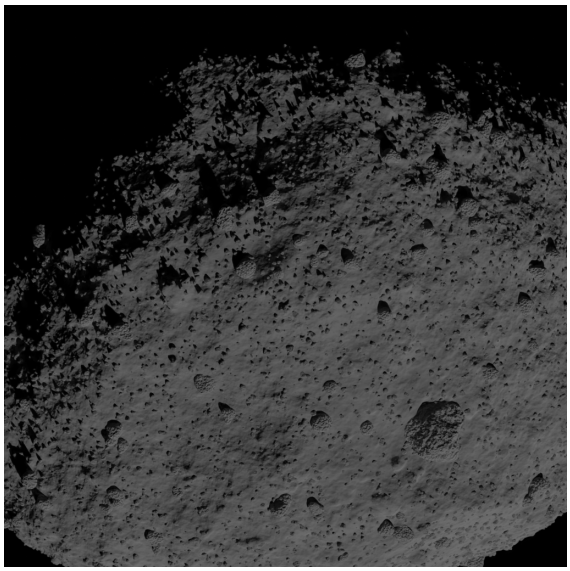

Figure 1. Example of the simulated images used in the image processing pipeline.

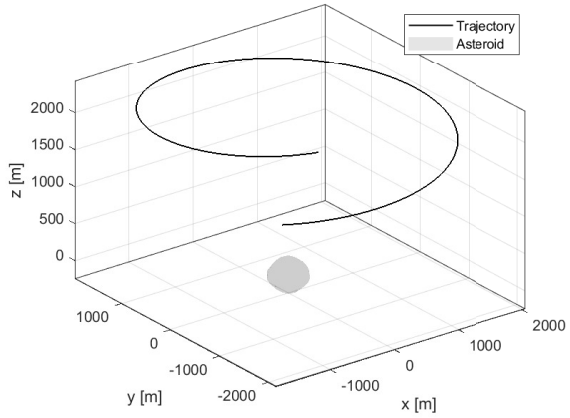

Figure 2. Spacecraft trajectory in the asteroid-fixed frame and asteroid shape model.

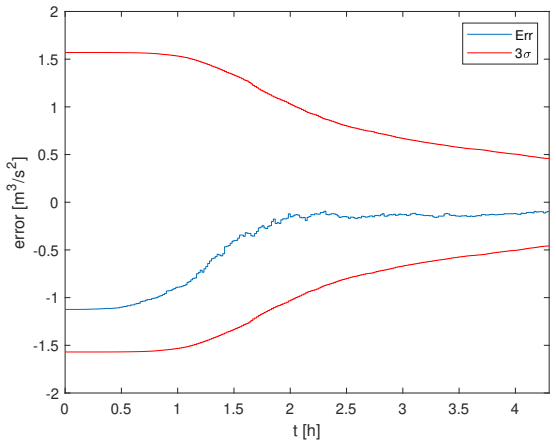

Figure 3. EKF gravitational parameter estimation error and formal uncertainty.

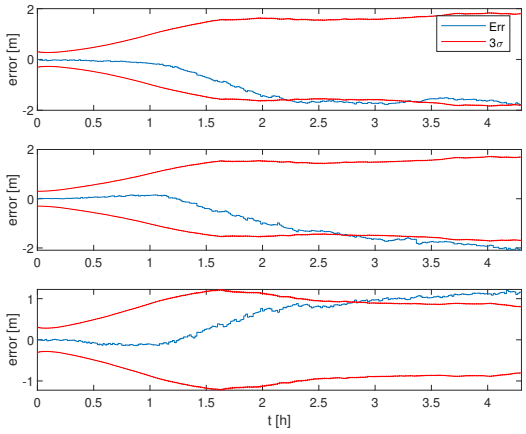

(a) Position error.

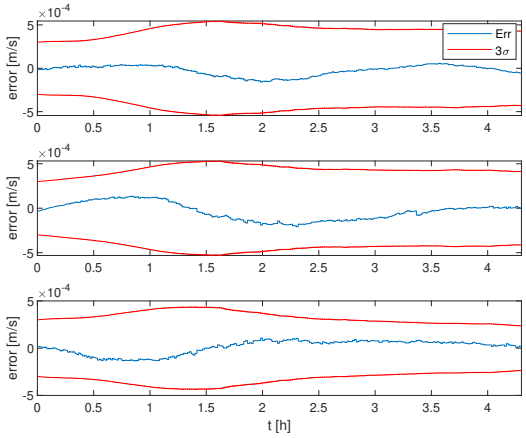

(b) Velocity error.

Figure 4. EKF position and velocity estimation error and formal uncertainty.

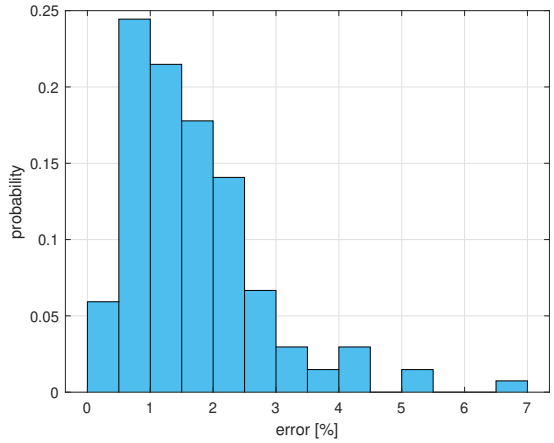

Figure 5. Histogram of the shape reconstruction error, shown as percentage of Bennu's mean radius.